Appl. Phys. B 54, 544–551 (1992)

Applied Physics B Photophysics and Laser Chemistry

The Physics of Pyroelectric Infrared Devices

S. Bauer, S. Bauer-Gogonea, and B. Ploss

Institut für angewandte Physik der Universität (TH) Karlsruhe, Kaiserstrasse 12, W-7500 Karlsruhe, Fed. Rep. Germany

Received in revised form 23 December 1991/Accepted 20 February 1992

Abstract. The absorption of radiation with pyroelectric detectors and the thermal properties of these devices are discussed using a simple physical picture – the physics of waves. Considered are the reflection, transmission and interference of electromagnetic and of thermal waves within the pyroelectric sensor arrangement. In particular, thin metal films, quarter wavelength structures, and anti-reflection coatings on metal films as absorber structures are discussed. The effect of the substrate on the pyroelectric response is treated and new figures of merit are introduced for the comparison of sensor materials which are mounted on a heat sink.

PACS: 07.62.+s, 85.50.Ly

A pyroelectric radiation detector consists of a pyroelectric element, covered by two metal electrodes and, in general, a radiation absorbing layer on top of the sensor and a substrate at the back of the sensor, as shown schematically in Fig. 1. The sensor element is heated by the absorption of intensity modulated light. This causes a temperature increase of the pyroelectric film, which is detected either as a voltage or as a current signal.

For a pyroelectric sensor element having an absorber structure and a substrate with thermal capacities negligible compared to that of the pyroelectric layer, the pyroelectric current is given by [1]:

$$I_{\sim} = \frac{\eta_{\sim} A p}{c \varrho d} \tag{1}$$

with:
η : absorption
$j_{\sim}$: incident intensity of the modulated light
A : sensor area
p : pyroelectric constant
c : specific heat
ϱ : density
d : thickness of pyroelectric element

independent of the modulation frequency. However, in the case of an absorber structure and a substrate with thermal capacities comparable to that of the pyroelectric element, the calculations become more difficult, as now not only the pyroelectric element is heated by the incident radiation, but also the whole multilayer structure of Fig. 1. If the incident radiation is not absorbed solely by the absorber structure, it is necessary to take into account the optical properties of the complete multilayer of Fig. 1. As the thermal properties of each layer are also different, it seems to be a difficult task to calculate the temperature increase within the multilayer.

While the general features of pyroelectric detectors can be found in the review article of Whatmore [2], the idea of this theoretical paper is a simple discussion of the optical and thermal effects that enter into the response of the device. For this purpose a simple physical picture is used – well known in the field of photoacoustics [3] – the physics of electromagnetic and thermal waves and their reflection, transmission, and interference within the multilayer of Fig. 1.

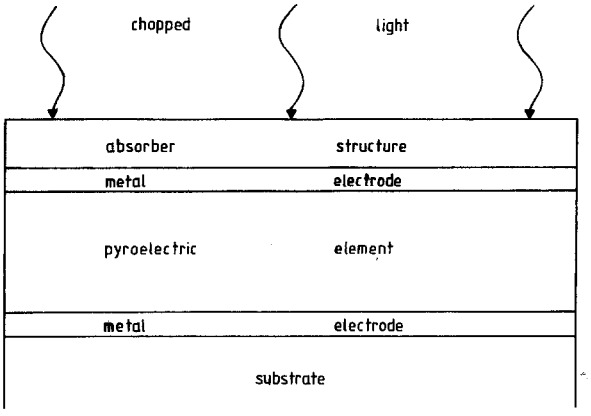

Fig. 1. Schematic view of a pyroelectric sensor element. The sensor consists of the pyroelectric element, covered by two electrodes, of an absorber structure, and a substrate

The paper is organized as follows. In the first section, a short derivation of the formulae for the multiple beam interference with a plane parallel plate is given. In the following sections it is shown that these formulae are sufficent to solve a variety of the physical problems associated with a pyroelectric infrared device. In the second section, the problem of the construction of an absorber structure with small thermal capacity is discussed. The problems that occur with thin metal film absorbers are discussed, as well as the fact that there are differences in the optical behaviour of the two typical classes of materials used for pyroelectric sensors: ionic crystals and ferroelectric polymers. Special solutions for the wavelength range from 9 μm to 15 μm, as the quarter wavelength structure of Parsons and Pedder [4] and anti-reflection coatings on metal films, as introduced by Yoshida for solar selective absorbers [5], are discussed. In the final section, the effect of the substrate on the pyroelectric response is treated and new figures of merit are introduced for the comparison of sensor materials which are mounted on a heat sink.

1 Multiple Beam Interference with a Plane Parallel Plate

For the following discussion, the transmission and reflection for a plane parallel plate henceforth called Fabry-Perot arrangement is needed. Figure 2 is illustrating the Fabry-Perot resonator and the first few contributions to the infinite series of partially reflected and transmitted waves generated by internal reflection in this lamellar specimen [6]. r_{ij} and t_{ij} denote the amplitude reflection and transmission coefficients for waves incident from medium i onto the interface to medium j. Φ denotes the phase and the attenuation factor of the wave travelling through the lamellar of thickness d. The concrete meaning of r_{ij}, t_{ij}, and Φ is specified in the following sections.

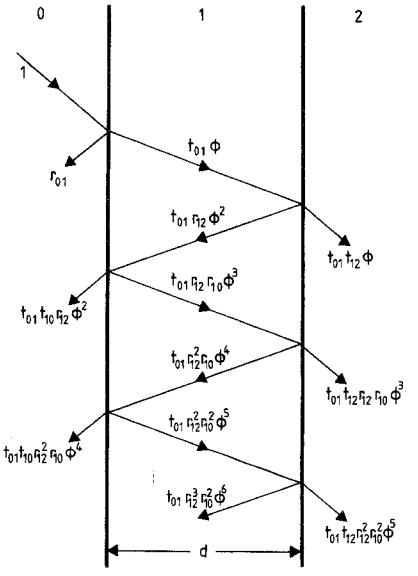

Fig. 2. Illustration of the first few contributions to the infinite series of partially reflected and transmitted waves, generated by internal reflection in a lamellar specimen

The amplitude reflection r and transmission t for this device are given by the infinite series:

$$\begin{aligned} r &= r_{01} + t_{01}t_{10}r_{12}\Phi^2[1 + r_{01}r_{12}\Phi^2 + (r_{01}r_{12}\Phi^2)^2 + \dots] \\ &= r_{01} + \frac{t_{01}t_{10}r_{12}\Phi^2}{1 - r_{01}r_{12}\Phi^2}, \\ t &= t_{01}t_{12}\Phi[1 + r_{01}t_{12}\Phi^2 + (r_{01}r_{12}\Phi^2)^2 + \dots] \\ &= \frac{t_{01}t_{12}\Phi}{1 - r_{01}r_{12}\Phi^2}. \end{aligned} \tag{2}$$

The amplitude of the resulting wave $\alpha(x)$ within the lamellar specimen is given by

$$\begin{aligned} \alpha(x) &= t_{01}\alpha_+(x)\,[1 + r_{12}r_{10}\Phi^2 + (r_{12}r_{10}\Phi^2)^2 + \dots] \\ &\quad + t_{01}t_{12}\Phi\alpha_-(x)\,[1 + r_{12}r_{10}\Phi^2 + (r_{12}r_{10}\Phi^2)^2 + \dots] \\ &= \frac{t_{01}\alpha_+(x)}{1 - r_{12}r_{10}\Phi^2} + \frac{t_{01}t_{12}\Phi\alpha_-(x)}{1 - r_{12}r_{10}\Phi^2} \end{aligned} \tag{3}$$

with

$\alpha(x)$: resulting normalized wave amplitude,
$\alpha_+(x)$: normalized wave travelling in the $+x$ direction,
$\alpha_-(x)$: normalized wave travelling in the $-x$ direction.

2 Absorber Structures with Small thermal Capacity

For thermal detectors an absorber is needed which should absorb 100% of the incident radiation over a large range of wavelengths. However, the thermal capacity of the absorber should be small compared to the sensor element, e.g., the pyroelectric slab. The discussion of metal black coatings is omitted, as they are treated in detail in the literature [7, 8] and because black paints have a high thermal capacity and metal blacks represent fragile absorber systems. For the Golay cell, thin free-standing metal films are known to be good, broadband absorber structures with minimal thermal capacity [9]. As known from Woltersdorf [10] the maximal absorption for a free standing film is 50%, the rest of the incident light being reflected (25%) and transmitted (25%). Hilsum [11] and Silberg [12] have shown that, as expected, the absorption of a metal film on a dielectric substrate is influenced by the substrate. In their considerations it is assumed that the dielectric properties of the substrate are described by a real, frequency-independent refractive index, an assumption which is not justified for pyroelectric materials in the IR wavelength region. It is shown that there are differences in the absorption for the two typical classes of pyroelectric materials used, e.g., ionic crystals and polymers. A special solution suitable for ionic ferroelectrics has been demonstrated by Parsons and Pedder [4], who use a quarter wavelength structure at 10 μm. Another possibility has been proposed by Yoshida [5] for solar selective absorbers: anti-reflection coating on a metal film. It is shown that it is possible to realize anti-reflection coatings on a metal film even in the IR wavelength region from 8–15 μm. The discussion shows why the experimental results of Stuhec and Zscheyge [13], with various thin metal films on KBr substrates, cannot be used for the construction of an absorber for a pyroelectric sensor. Thus, the construction of a very thin and broadband absorber still represents a problem for pyroelectric sensors.

For a further recent work on absorbers for thermal sensors see the work of Hadni and Gerbaux [14].

2.1 Optical Properties of Pyroelectric Materials

For pyroelectric sensor applications two classes of materials are used: ionic crystals (typical examples are $LiTaO_3$ and $LiNb_3$) and molecular crystals or polymers (typical examples are PVDF and its copolymers and recently some nylon compounds).

For the two classes of materials, characteristic differences in the complex dielectric function occur. The dielectric function is described by a sum of Drude-Lorentz oscillators:

$$\tilde{\varepsilon} = \varepsilon_1 + i\varepsilon_2 = \varepsilon_\infty + \sum_n \frac{\Omega_{an}^2}{-\omega^2 + \Omega_{on}^2 - i\omega\Omega_{\tau n}} \quad (4)$$

with:
Ω_{an}: oscillator strength,
Ω_{on}: resonance frequency,
$\Omega_{\tau n}$: damping frequency.
The ionic crystals are characterized by few, strong and broad oscillators, the polymers by many small, narrow oscillators; more than that, for ionic crystals there exist wavelength regions with $\varepsilon < 0$.

As a typical example, Fig. 3 shows the dielectric function of $LiNbO_3$, the parameters for the calculations are gained from the work of Barker and Loudon [16]. Between 9 µm and 17 µm it can be seen that $\varepsilon_1 < 0$; this includes the most important wavelength regions used for pyroelectric IR sensor applications. Figure 4 shows the dielectric function of

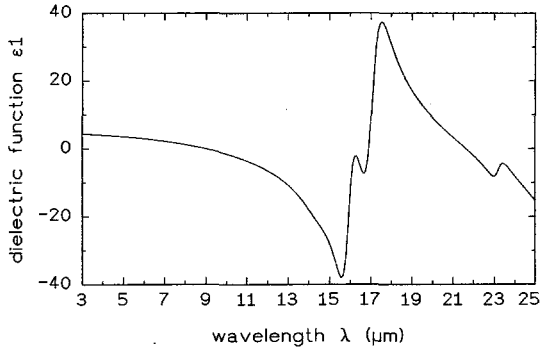

Fig. 3. Real part ε_1 of the dielectric function $\tilde{\varepsilon} = \varepsilon_1 + i\varepsilon_2$ of $LiNbO_3$ from 3 µm to 25 µm

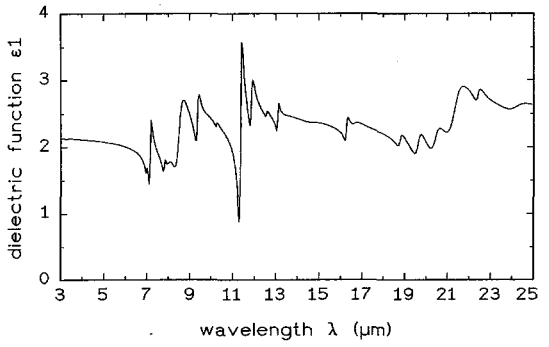

Fig. 4. Real part ε_1 of the dielectric function of PVDF from 3 µm to 25 µm

Table 1. Optical properties of PVDF ($\varepsilon_\infty = 2.16 + i0.001$)

n	Ω_{on}/cm^{-1}	Ω_{an}/cm^{-1}	$\Omega_{\tau n}/cm^{-1}$
1	3012.7	50	30
2	2979.4	17	7
3	2297.2	25	55
4	1431.4	60	15
5	1400	160	18
6	1282	60	12.5
7	1250	150	65
8	1178.25	295	65
9	1070	118	17
10	1030.9	73	60
11	975.8	25	7
12	880	150	9
13	843	83	10.5
14	796.4	25	6.5
15	764.6	40	5
16	746.3	55	60
17	676.9	30	36
18	615.2	34	5.2
19	601.2	32	18
20	532.7	27	6.5
21	510.1	45	10
22	489.8	60	15
23	469.1	92	21
24	445.9	22	5
25	412.7	35	20
26	372.7	16	10
27	352	27	15
28	74.1	45	35

PVDF. The parameters are obtained from a Drude-Lorentz fit of a transmission spectrum of a 9 µm thick PVDF film and given in Table 1. In contrast to the case of $LiNbO_3$, $\varepsilon_1 > 0$ for PVDF, within the whole wavelength range. It is to be expected that these characteristic differences in the dielectric functions also influence the optical absorption of a pyroelectric sensor covered with two thin metal electrodes.

In the following, it is shown that for ionic crystals the absorption of the sensor is quite low in wavelength regions with $\varepsilon_1 < 0$. This is in contrast to ferroelectric polymers where the absorption is always greater than 50%.

2.2 The Absorption of Thin Metal Films on Pyroelectric Substrates

Figure 5 shows the electric and magnetic field for the system: dielectric material with complex refractive index $\tilde{n}_1$, thin metal film with conductivity σ and thickness d and dielectric material with complex refractive index $\tilde{n}_2$. The thickness of the metal film is assumed to be smaller than the wavelength λ of the radiation and the skin depth δ. This condition is well fulfilled for the infrared radiation region considered, as the typical metal film thicknesses required are approximately a few 100 Å. Thus, the electric and magnetic fields have no spatial dispersion over the film thickness. The amplitude reflection and transmission coefficients follow from the boundary conditions for the fields [15]

$$\begin{aligned} E_i + E_r &= E_t, \\ H_i - H_r &= H_t + \sigma d E_t, \end{aligned} \quad (5)$$

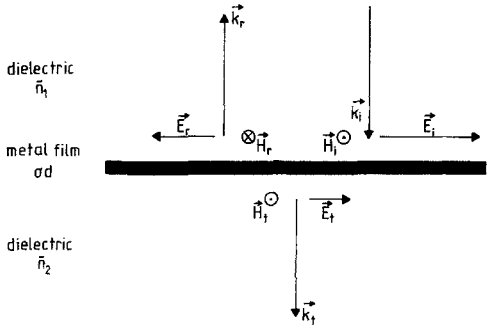

Fig. 5. Incident, transmitted and reflected electric and magnetic fields at an interface between two dielectric materials with indices of refraction $\tilde{n}_1$ and $\tilde{n}_2$ and a thin metal sheet of conductivity σ and thickness d

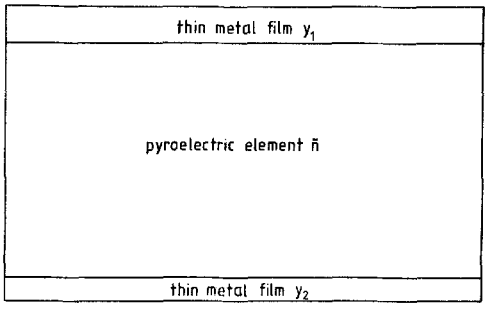

Fig. 6. Schematic view of a pyroelectric sensor with the minimum thermal capacity possible. The sensor is covered by two metal electrodes, specified by y_1 and y_2

with $H = \tilde{n}\varepsilon_0 c_0 E$, ε_0 denotes the permittivity of vacuum and c_0 the vacuum velocity of light, and are given by:

$$r_{12} = \frac{E_r}{E_i} = -\frac{\tilde{n}_2 - \tilde{n}_1 + y}{\tilde{n}_2 + \tilde{n}_1 + y},$$
$$t_{12} = \frac{E_t}{E_i} = -\frac{2\tilde{n}_1}{\tilde{n}_2 + \tilde{n}_1 + y}, \tag{6}$$

with

$$y = \frac{\sigma d}{\varepsilon_0 c}. \tag{7}$$

For an unsupported thin metal film in vacuum, the absorption A is given by

$$A = 1 - |r|^2 - |t|^2 = \frac{4y}{(2+y)^2} \tag{8}$$

and with $y = 2$ one gets the result for a Woltersdorff-film [10]. This corresponds to a square resistance of the film of $R = 188\,\Omega$, which is half the impedance of vacuum $Z_0 = \sqrt{\mu_0/\varepsilon_0} = 377\,\Omega$. Some important conclusions can be drawn from (6, 7):

1. The result of a maximum absorption of 50% for a thin metal film with $y = 2$, is valid only for the unsupported metal film.

2. It is possible to realize a zero reflection for the arrangement, if the refractive indices are real and if $\tilde{n}_1 > \tilde{n}_2$, then $y = \tilde{n}_1 - \tilde{n}_2$.

3. The reflection coefficient for the system: vacuum–metal film–dielectric is high, if either the real or the imaginary part or both parts of the refractive index of the dielectric are high. This occurs near the resonance frequency of a strong, broad Lorentz-oscillator, especially in the regions with $\varepsilon_1 < 0$.

Figure 6 shows the arrangement for a pyroelectric sensor, which yields the minimum thermal capacity. The needed reflection and transmission coefficients are calculated according to (6, 7), and the phase and attenuation factor Φ is given by

$$\Phi = \mathrm{e}^{\mathrm{i}k_0\tilde{n}d} \tag{9}$$

with k_0 the vacuum wave-vector of the incident light. With (2) the absorption of the arrangement of Fig. 6 is calculated. Figure 7a shows the absorption of a 25 µm $LiNbO_3$ crystal at normal incidence from 3 µm to 25 µm, as calculated from the complex dielectric constant given in the work of

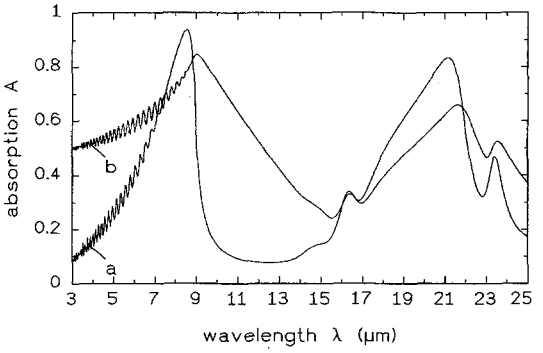

Fig. 7. Calculated absorption for several arrangements from 3 µm to 25 µm. *a* 25 µm thick $LiTaO_3$ crystal. *b* Woltersdorff-layer, 25 µm thick $LiTaO_3$ crystal, impedance matching layer

Barker and Loudon [16]. There is a strong absorption peak in the region near 9 µm, a wavelength-range which is most important for infrared sensors, as the maximum of the blackbody spectrum at 300 K occurs at 10 µm. Figure 7b shows the calculated absorption of a 25 µm thick $LiNbO_3$ crystal, covered by a Woltersdorff-layer with $y_1 = 2$ and at the back an impedance matching layer with $y_2 = 1.12$. The refractive index of $LiNbO_3$ is $n = 2.12$ at 3 µm. However, it is not possible to get a wavelength independent absorption in the 10 µm region, as in this region the dielectric function has a negative real part. As shown before, this will lead to a high reflection coefficient for the arrangement. In this wavelength range it is sufficient to consider the reflection only, as the radiation entering the crystal is strongly attenuated after traversing the 25 µm thick crystal. It must be concluded that thin metal films can be problematic if used a broadband absorber structures for pyroelectric detectors with ionic crystals, in cases where the detector material shows strong Lorentz-oscillators in the near infrared. For this reason the results of Stuhec and Zscheyge [13] cannot be used for the construction of an absorber for pyroelectric sensors, as they made experiments with thin metal films on the transparent substrate KBr.

Figure 8a shows the absorption of a 25 µm thick PVDF film at normal incidence from 3 µm to 25 µm with the oscillator parameters as given in Table 1. In the region between 9 µm and 15 µm many strong narrow absorption peaks occur causing the absorption to vary in this region between 20% and 95%. Figure 8b shows the calculated absorption of a 25 µm thick PVDF film, covered with a Woltersdorff-layer

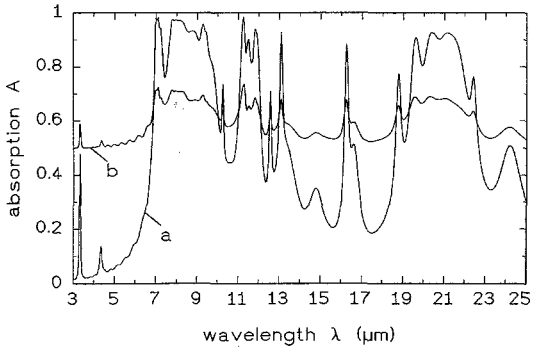

Fig. 8. Calculated absorption for several arrangements from 3 μm to 25 μm. *a* 25 μm thick PVDF film. *b* Woltersdorff-layer – 25 μm thick PVDF film, impedance matching layer

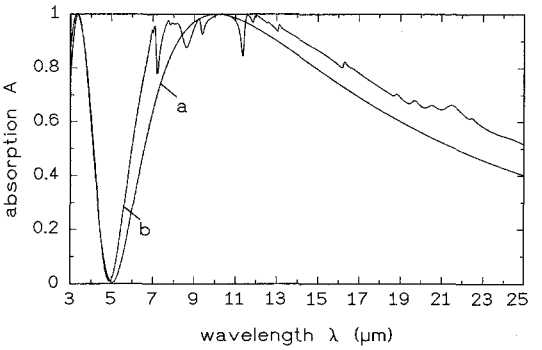

Fig. 10. *a* Absorption of the structure of Fig. 9 with polyimide. The absorption is zero for 5 μm and 100% for 10 μm. *b* Absorption of the structure of Fig. 9 with PVDF

with $y_1 = 2$ and at the back with an impedance matching layer with $y_2 = 0.44$. The refractive index of PVDF at 3 μm is $n = 1.44$. In contrast to the case of $LiNbO_3$, the absorption in the region from 3 μm to 25 μm is relatively high (average absorption of 60% of the incoming radiation) and has a maximal variation of 20%.

2.3 Quarter Wavelength Structures and Anti-Interference Coatings on Metals

In the last section it was shown that thin metal films give inherent problems if used as absorber structures for thermal sensors as either the absorption shows strong variations over the IR wavelenght region of interest or the absorption is only about 50% of the incoming radiation. A solution is the development of absorber structures, which have an absorption of nearly 100% in the infrared region from 9 μm to 15 μm. Two possible solutions are discussed, a quarter wavelength structure at 10 μm [4] and an anti-reflection coating for the metal electrode of the pyroelectric sensor element.

2.3.1 Quarter-Wavelength Structure at 10 μm. Parsons and Pedder [4] consider an arrangement, which consists of a Ni–Cr layer with $y_1 = 1$, a 1.4 μm thick Polyimide dielectric film, which has an refractive index of $\tilde{n} = 1.8$ in the wavelength range of interest, and of a titanium reflector with $y_2 \approx \infty$ on the back, as shown schematically in Fig. 9.
By using the reflection and transmission coefficients calculated according to (6), with Φ as given by (9) and with (2), the formulae of Hilsum [11] and Silberg [12] can be rederived in a very simple way. Hilsum [11] only considered the supported metal film and the system: metal film, dielectric, metal film with the metal films chosen so that $y_1 = y_2$. Silberg considered the more general arrangement of Fig. 9, with an arbitrary resistance of the reflector. With $\Phi = i$ the formula, as given by Silberg [12], follows:

$$A = \frac{4y_1(y_2+1)^2 + n^2 y_2}{[(y_1+1)(y_2+1)+n^2]^2} . \tag{10}$$

Silbergs formula allows a discussion of the effect of the resistance of the reflector on the maximum absorption of the device of Fig. 9. For $y_1 = 1$ and $y_2 = \infty$ the maximum absorption of the arrangement is 100% at 10 μm. Figure 10a shows the result of a calculation. It is in good agreement with experimental data in the wavelength range from 9 μm to 15 μm, as shown by Turnbull [17]. However, the absorption would be zero at 5 μm. This shows that the device is a good absorber only from 9 μm to 15 μm. With a thickness of 1.4 μm, the absorber structure has a thermal capacity which is low enough for most applications.

It is possible to realize a quarter wavelength structure with ferroelectric polymers. The thickness needed for the pyroelectric films is approximately $d = 1.7$ μm. The absorption of this arrangement is shown in Fig. 10b. In this case the pyroelectric sensor is a part of the absorber structure.

2.3.2 Anti-Reflection Coating on a Metal Film. Yoshida [5] considered the problem of an anti-reflection coating for a metal film for a solar selective absorber. The arrangement is shown schematically in Fig. 11. It is assumed that the metal is thick enough, so that infrared radiation, which enters the metal, is completely absorbed. Then the formulas for the Fabry-Perot resonator hold. From these, it is shown in [5]

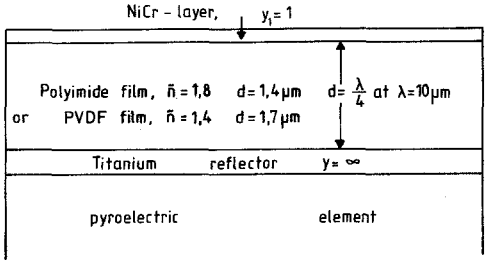

Fig. 9. Quarter-wavelength structure of Parsons and Pedder [4]. The structure can be realized with polyimide (a) but also with a pyroelectric polymer as PVDF (b)

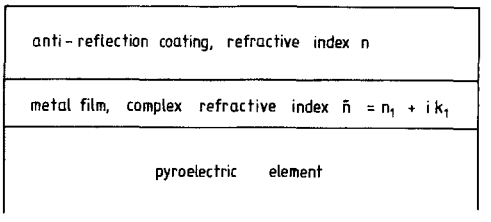

Fig. 11. Anti-reflection coating for the metal electrode of a pyroelectric element. The metal electrode is assumed to be thick enough to absorb all the radiation which enters the metal

that it is possible, to make an anti-reflection coating on a metal film for the wavelength λ, if the following conditions hold.

The thickness of the anti-reflection coating is given by:

$$nd = \frac{\lambda}{2}\left\{2 - \frac{1}{2\pi}\tan^{-1}\left[-\frac{2nk_1}{(n^2 - n_1^2 - k_1^2)^2}\right]\right\} \tag{11}$$

and to achieve 100% absorption the refractive index should be chosen to be

$$n = \sqrt{n_1 + \frac{k_1^2}{n_1 - 1}}\,. \tag{12}$$

The main problem for the infrared region is to find a combination of materials which satisfy these requirements at least approximately [18]. Materials which can be used for the infra-red are Cr, Bi, Sb (n = 4-6.5), Te(n = 5.5-6.5), and Se (n = 3.5-4.5). With combinations of these materials it is possible to satisfy (12) approximately. For good conducting metals, like Ag and Al, it is not possible to find materials for an anti-reflection coating. Experimentally realized anti-reflection coatings showed, that a maximum absorption of 70% is possible for the system 0.4 µm thick Te film on a 0.6 µm thick Cr film. This absorber structure can be easily prepared and has similar properties as the absorber structure of Parsons and Pedder [4]. An advantage of the anti-reflection coating is that the electrode and the anti-reflection coating can be produced within the same process, while the production of quarter-wavelength structures requires an additional preparation process.

3 The Influence of the Substrate on the Pyroelectric Response and Figures of Merit

For any homogeneously poled pyroelectric sensor of Fig. 1, it can be shown that the pyroelectric current response is proportional to the time derivative of the average temperature of the pyroelectric element [1]:

$$I_\sim = \frac{Ap}{d}\frac{\partial}{\partial t}\int_0^d \Delta T_\sim(x,t)dx \tag{13}$$

with $\Delta T_\sim(x,t)$ the temperature increase in the pyroelectric element.

Usually the pyroelectric voltage is recorded using a FET as an impedance converter. For harmonic excitation and for frequencies higher than the reciprocal electrical RC-time, the amplitude of the pyroelectric voltage is given by:

$$|U_\sim| = \frac{|I_\sim|}{\omega(C_\mathrm{P} + C_\mathrm{A})} \tag{14}$$

with:

$U_\sim$: pyroelectric voltage signal,
C_P: electric capacity of the pyroelectric element,
C_A: input capacity of the impedance matching FET.

The voltage sensitivity R_V is defined as the quotient of the pyroelectric voltage signal and the incident radiation power.

Untill now, only the optical problems of the device are discussed. To treat the effect of the substrate on the pyroelectric response, it is assumed that a very thin (as compared with the pyroelectric element) absorber is used and that the absorption takes place only in the absorber structure. Figure 12a, b show the two possible extreme cases: no substrate, e.g., a free-bearing mounting of the sensor and a thick, highly thermally conducting substrate, e.g., a sensor mounted on a heat sink. The assumption of a heat sink is justified for integrated pyroelectric sensors, for which the pyroelectric element is directly deposited on silicon chips, as described by Bauer and Ploss [19]. As the thermal conductivity of the silicon chip is much higher than that of the pyroelectric element, the silicon chip is working as a heat sink at the back of the pyroelectric element in a good approximation [20].

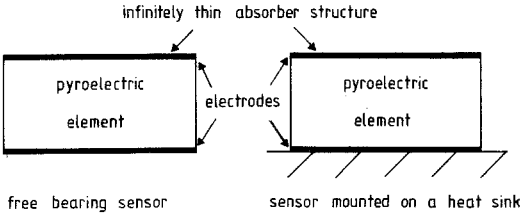

Fig. 12. Schematic view of the two arrangements discussed. **a** Sensor mounted free-bearing. **b** Sensor mounted with its back surface on a heat sink

For the calculation of the pyroelectric response, it is necessary to solve the heat conduction equation for the two arrangements of Fig. 12a, b. The general solution of the heat conduction equation is a thermal wave and given by

$$\Delta T_\sim(x,t) = \Delta T_\sim(x=0)\mathrm{e}^{-(1+\mathrm{i})kx+\mathrm{i}\omega t} \tag{15}$$

with:

$k = \sqrt{\omega/2D}$: wave vector of the thermal wave,
$D = \kappa/c\varrho$: thermal diffusivity of the pyroelectric element,
κ: thermal conductivity,
$c\varrho$: specific heat per volume.

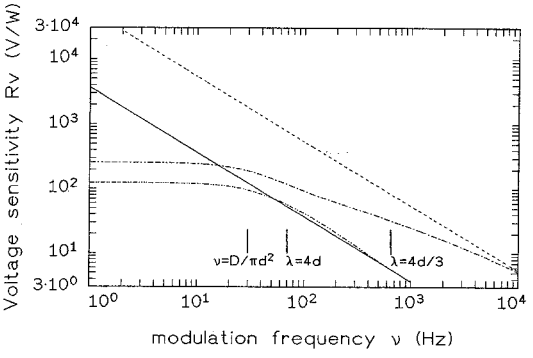

Fig. 13a–d. Voltage sensitivity for a variety of sensor arrangements as a function of the modulation frequency: **a** Free-bearing 25 µm thick PVDF sensor (——). **b** 25 µm thick sensor mounted on a heat-sink (– · · –). The range of validity for the new figures of merit is marked by a dashed vertical line. Two solid vertical lines show the modulation frequencies, for which the wavelength of the thermal wave is given by $\lambda = 4d/3$ and $\lambda = 4d$. **c** Free-standing Parsons-Pedder structure (– – –). **d** Parsons-Pedder structure, thermally isolated from the silicon chip with a 25 µm thick polymer film (– · – ·)

At boundaries between materials of different thermal properties, thermal waves are reflected and transmitted. In [3] the reflection and transmission coefficients are given:

$$r_{ij} = \frac{\kappa_i k_i - \kappa_j k_j}{\kappa_i k_i + \kappa_j k_j}, \qquad t_{ij} = \frac{2\kappa_i k_i}{\kappa_i k_i + \kappa_j k_j}. \tag{16}$$

These are the analogues to the Fresnel equations for normal incidence, but unlike the optical case the thermal r_{ij} and t_{ij} are frequency independent real numbers.

For the two arrangements to be considered, the following approximations are made:
Free-bearing mounted sensor: $\kappa_0 \approx 0$, $\kappa_2 \approx 0$, $k_0 \approx 0$, $k_2 \approx 0$;
thus $r_{12} = 1$.
Sensor mounted on the heat sink: $\kappa_0 \approx 0$, $\kappa_2 \approx \infty$, $k_0 \approx 0$, $k_2 \approx \infty$;
thus $r_{12} = -1$,
and $r_{10} = 1$, $\Phi = \mathrm{e}^{-(1+\mathrm{i})kd}$, $\alpha_+ = \mathrm{e}^{-(1+\mathrm{i})kx+\mathrm{i}\omega t}$, $\alpha_- = \mathrm{e}^{(1+\mathrm{i})kx+\mathrm{i}\omega t}$ for both cases.

Using these approximations, the temperature distribution within the film is evaluated according to (3) [it is assumed, that the thermal wave starts at $x = 0$ in the pyroelectric slab, thus we neglect t_{01} in (3)]. With the temperature distribution, the voltage sensitivity follows:

Free-bearing mounted sensor:

$$R_V = \frac{p}{(C_A + C_P)\omega c\varrho d};$$

Sensor mounted on a heat sink:

$$R_V = \frac{p}{(C_A + C_P)\omega c\varrho d} \frac{\cosh(1+\mathrm{i})kd - 1}{\cosh(1+\mathrm{i})kd}. \tag{17}$$

Figure 13 shows the result of a calculation for the voltage sensitivity R_V of the arrangements. A 25 µm thick PVDF films is used as the pyroelectric element. The parameters for the calculation are: $p = 25\,\mu\mathrm{C/m^2K}$, $C_A + C_P = 18\,\mathrm{pF}$, $c\varrho = 2.4\,\mathrm{J/cm^3\,K}$, $\kappa = 0.14\,\mathrm{W/mK}$. At high modulation frequencies both sensor arrangements behave in the same way. This is simply understood, as for high modulation frequencies the thermal wave incident from the absorber is strongly attenuated within the pyroelectric material, and thus, interference effects vanish. In [21] it is shown that within the modulation frequency range according to $4d/3 < \lambda < 4d$,, the pyroelectric response of the sensor coupled to the heat sink exceeds the response of the respective free-bearing sensor. The position of these frequencies are marked by the solid vertical lines in Fig. 13. At low modulation frequencies the response of both arrangement differs. In [20] it is shown that pyroelectric materials mounted on a heat sink are better characterized by new figures of merit (foms) in the flat region of the voltage sensitivity for $\omega < 2D/d^2$:

$$\text{Voltage fom, heat sink: } F_{V,\,\mathrm{sink}} = \frac{p}{\varepsilon_0 \varepsilon \kappa}; \tag{18}$$

$$\text{Current fom, heat sink: } F_{I,\,\mathrm{sink}} = \frac{p}{\kappa}; \tag{19}$$

Signal-to-Noise fom, heat sink:

$$F_{N,\,\mathrm{sink}} = \frac{p}{\kappa\sqrt{\varepsilon_0 \varepsilon \tan\delta}}; \tag{20}$$

with ε the dielectric constant and $\tan\delta$ the dielectric loss of the pyroelectric material.

It can be seen that pyroelectric polymers are very attractive for applications in integrated pyroelectric sensors, due to the low thermal conductivity. The best suited material is TGS.

4 Improved Pyroelectric Sensor Design

For the optimization of a pyroelectric sensor design several aspects have to be considered. The heat capacity of the total arrangement of sensor must be small, just so the heat loss to the surroundings. The absorption for incoming radiation must be high, and also the pyroelectric coefficient. With the results of the preceeding sections, an improved pyroelectric sensor arrangement with the material PVDF is discussed.

Using a PVDF film with a thickness of 1.7 µm it is possible to realize a Parsons-Pedder structure with the pyroelectric film as a part of the absorber structure. Though the pyroelectric film is only 1.7 µm thick, the heat capacity of the sensor is dominated by the heat capacity of the pyroelectric film. Due to the low heat capacity of the sensor, the voltage sensitivity of the free-bearing Parsons-Pedder arrangement is an order of magnitude higher than that of a free-bearing 25 µm thick PVDF sensor, if the same pyroelectric coefficient is achieved with the 1.7 µm thick PVDF film as with the 25 µm thick PVDF film. Figure 13 shows the calculated voltage sensitivity of the free-bearing 1.7 µm thick Parsons-Pedder structure (c) compared with a 25 µm thick PVDF film (a). In both cases a relative high load capacity of 40 pF of the amplifier circuit is assumed.

With integrated sensors the thermal properties of the free bearing structure can be realized approximately, if the silicon beneath the sensor element is removed by etching, as shown in Fig. 14a. For a thick silicon chip a thermal isolation of the pyroelectric film from the chip via a 25 µm thick PVDF layer is shown in Fig. 14b. The calculated voltage sensitivity for this arrangement is shown in Fig. 13d in comparison with a 25 µm thick PVDF sensor film directly deposited on the silicon chip (Fig. 13b). At low modulation frequencies an

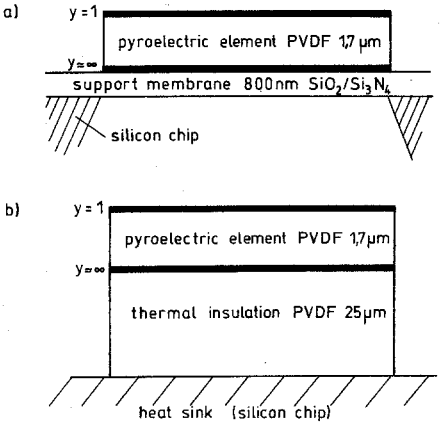

Fig. 14. Two optimal design solutions of pyroelectric infrared sensors with polymers. **a** Free-standing Parsons-Pedder structure, approximately realized on a silicon chip by removing the silicon beneath the sensor. **b** Parsons-Pedder structure thermally isolated from the silicon chip with a 25 µm thick polymer film

improvement by a factor of two is gained, while at high modulation frequencies the performance of the free-bearing Parsons-Pedder structure is approximated.

5 Conclusion

It is shown that several problems of the physics of pyroelectric devices (absorber structures and the effect of the substrate on the pyroelectric response) can be discussed by the same physical picture – the physics of electromagnetic and thermal waves and the formulae for the Fabry-Perot resonator. Thin metal films have severe problems, if used as absorbers for pyroelectric sensors. Good solutions in the wavelength range from 9 μm to 15 μm are a quarter-wavelength structure or an anti-reflection coating for the metal electrode of the pyroelectric element. For the discussion of the merit of pyroelectric materials mounted on a heat sink, new figures of merit are used. Suggestions for the design of improved pyroelectric sensors are given. For the simulation and the optimization of and real sensor element, however, a matrix method for the electromagnetic problem and for the thermal problem is required (this is well known for photoacoustic arrangements [3]).

Acknowledgements. The authors gratefully acknowledge the stimulating interest of Prof. Dr. W. Ruppel, Dr. habil. P. Würfel, and Dipl. Phys. R. Fettig. Financial support of the Deutsche Forschungsgemeinschaft is gratefully acknowledged for S. B.; Financial support of the DAAD is gratefully acknowledged for S.B.G.

References

1. S.B. Lang, D.K. DasGupta: J. Appl. Phys. **59**, 215 (1986)
2. R.W. Whatmore: Rep. Prog. Phys. **49**, 1335 (1986)
3. P. Grosse, R. Wynands: Appl. Phys. B **48**, 59 (1989)
4. A.D. Parsons, D.J. Pedder: J. Vac. Sci. Technol. A **6**, 1686 (1988)
5. S. Yoshida: Thin Solid Films **56**, 321 (1979)
6. M. Born, E. Wolf: *Principles of Optics* (Pergamon, New York 1959) p. 322
7. W.R. Blevin, J. Geist: Appl. Opt. **13**, 1171 (1974)
8. D.B. Betts, F.J.J. Clarke, L.J. Cox, J.A. Larkin: J. Phys. E: Sci. Instrum. **18**, 689 (1985)
9. M.J. Golay: Rev. Sci. Instrum. **18**, 357 (1947)
10. W. Woltersdorff: Z. Phys. **91**, 230 (1934)
11. C. Hilsum: J. Opt. Soc. Am. **44**, 188 (1954)
12. A. Silberg: J. Opt. Soc. Am. **47**, 575 (1957)
13. H. Stuhec, W. Zscheyge: Exp. Tech. Phys. **32**, 325 (1984)
14. A. Hadni, X. Gerbaux: Infrared Phys. **30**, 465 (1990)
15. S.W. McKnight, K.P. Stewart, H.D. Drew, K. Moorjani: Infrared Phys. **27**, 327 (1987)
16. A.S. Barker, Jr., R. Loudon: Phys. Rev. **158**, 433 (1967)
17. A.A. Turnbull: Proc. SPIE Vol. **588**, 38 (1985)
18. P. Würfel: Private communication of unpublished results from the Diplomarbeit of R. Kilian, Karlsruhe (1982)
19. S. Bauer, B. Ploss: Ferroelectrics Lett. **9**, 155 (1989)
20. B. Ploss, S. Bauer: Sensors & Actuators A **25–27**, 407 (1991)
21. S. Bauer, B. Ploss: Sensors & Actuators A **25–27**, 417 (1991)